J|A|C|S ARTICLES

Published on Web 06/15/2009

High-Throughput Screening of Nanoparticle Catalysts Made by Flame Spray Pyrolysis as Hydrocarbon/NO Oxidation Catalysts

B. Weidenhof,[†] M. Reiser,[†] K. Stöwe,*[,†] W. F. Maier,[†] M. Kim,[‡] J. Azurdia,[‡] E. Gulari,[§] E. Seker,[§] A. Barks,[‡] and R. M. Laine*[,‡]

Lehrstuhl für Technische Chemie, Universität des Saarlandes, 66123 Saarbrücken, Germany, and Departments of Materials Science and Engineering and Chemical Engineering, University of Michigan, Ann Arbor, Michigan 48109-2136

Received November 21, 2008; E-mail: k.stoewe@mx.uni-saarland.de; talsdad@umich.edu

Abstract: We describe here the use of liquid-feed flame spray pyrolysis (LF-FSP) to produce high surface area, nonporous, mixed-metal oxide nanopowders that were subsequently subjected to high-throughput screening to assess a set of materials for deNO_x catalysis and hydrocarbon combustion. We were able to easily screen some 40 LF-FSP produced materials. LF-FSP produces nanopowders that very often consist of kinetic rather than thermodynamic phases. Such materials are difficult to access or are completely inaccessible via traditional catalyst preparation methods. Indeed, our studies identified a set of $Ce_{1-x}Zr_xO_2$ and $Al_2O_3-Ce_{1-x}Zr_xO_2$ nanopowders that offer surprisingly good activities for both NO_x reduction and propane/propene oxidation both in high-throughput screening and in continuous flow catalytic studies. All of these catalysts offer activities comparable to traditional Pt/Al_2O_3 catalysts but without Pt. Thus, although Pt-free, they are quite active for several extremely important emission control reactions, especially considering that these are only first generation materials. Indeed, efforts to dope the active catalysts with Pt actually led to lower catalytic activities. Thus the potential exists to completely change the materials used in emission control devices, especially for high-temperature reactions as these materials have already been exposed to 1500 °C; however, much research must be done before this potential is verified.

Introduction

In view of the issues of global warming and the energy crisis, the development of new, fuel economic vehicles that also offer low CO_2 emissions has become a major challenge of the modern mobile society. In addition, rising public concern about environmental hazards, and in particular NO_x pollutants and diesel soot, has led to strict automotive exhaust emission regulations.[1] Prompted by these concerns, the automobile industry has developed two engine technologies, the lean-burn direct injection gasoline and the common turbo-diesel engines. Both engine types offer excellent fuel economy compared to the classical gasoline engine but operate with higher air-to-fuel ratios ($\lambda > 1$). Under these so-called lean-burn conditions (excess oxygen), conventional three-way auto exhaust catalysts (TWCs) are incapable of completely reducing NO_x.

To overcome this problem, several promising techniques including NO_x storage reduction (NSR), selective catalytic reduction of NO_x by NH_3 or hydrocarbons (NH_3-SCR, HC−SCR), and nonthermal plasma have been proposed for abating NO_x emissions.[2,3] Among these techniques, the selective catalytic reduction of NO_x to N_2 by hydrocarbons offers the advantage that the unburnt hydrocarbons from combustion, possibly combined with purposely added hydrocarbons, can be used to reduce NO_x continuously without drastic modification of the engine management system.

This fact provides significant motivation for intense research in this area.[4,5] Different catalyst systems have been studied extensively for HC−SCR, targeting development of new catalyst materials that provide the desired NO_x control under lean-burn conditions. Such catalysts are also expected to display enhanced N_2 selectivity, improved low-temperature activity (a wider temperature range of operation), and high stability (H_2O or SO_2 poisoning, thermal degradation) under realistic exhaust gas conditions.[6] Among the systems investigated, several groups of metal oxide catalysts have attracted attention due to their high activity for NO_x reduction and good hydrothermal stability. Previous studies have emphasized the use of Co, Cu, Ag, Ga, In, and Sn containing oxides on alumina and other supports as active HC−SRC catalysts.[2] In addition, rare-earth-based materials, especially CeO_2 and CeO_2-ZrO_2 solid solutions, have been used widely in deNO_x and soot combustion systems due to their dynamic oxygen exchange capacity (OEC) involving the Ce^{4+}/

[†] Universität des Saarlandes.
[‡] Department of Materials Science and Engineering, University of Michigan.
[§] Department of Chemical Engineering, University of Michigan.

(1) Klingstedt, F.; Arve, K.; Eranen, K.; Murzin, D. Y. *Acc. Chem. Res.* **2006**, *39*, 273–282.
(2) Liu, Z.; Woo, S. I. *Catal. Rev.* **2006**, *48*, 43–89.
(3) Twigg, M. V. *Appl. Catal. B* **2007**, *70*, 2–15.
(4) Burch, R.; Breen, J. P.; Meunier, F. C. *Appl. Catal. B* **2002**, *39*, 283–303.
(5) Burch, R. *Catal. Rev.* **2004**, *46*, 271–334.
(6) Houel, V.; James, D.; Millington, P.; Pollington, S.; Poulston, S.; Rajaram, R.; Torbati, R. *J. Catal.* **2005**, *230*, 150–157.

Ce^{3+} redox couple as well as spillover of active oxygen.[7−14] Furthermore, for instance, Baiker et al.[15] and Kašpar et al.[16] showed that the thermal stability as well as the OEC of these solid solutions is improved by doping with small amounts of silica.

In contrast, these researchers report that doping with small amounts of alumina has little effect on OEC values. These doped nanopowders were made using LF-FSP processing. Baiker et al. do suggest formation of solid solutions with the silica or alumina dopants but do not further characterize silica or alumina species present. In the case of the alumina, this is understandable as the OEC activities are not comparable with the SiO_2-doped materials.

Several additional factors including support materials, catalyst composition, metal loading, calcination temperatures, preparation methods, and reaction conditions must be considered for the successful design of any new, high-activity catalyst systems. However, a vast number of possible elemental combinations with potential catalytic activity for the desired reactions remain to be explored. Unfortunately, the complexity of the variables involved limits the total number of systems that can be and have been investigated on various supports in the recent past.[2,17−21] Some of the reasons for this are as follows.

Heterogeneous catalysts are most often prepared using a set of standard methods including wet precipitation, sol−gel processing, solid-state reactions, and impregnation techniques (e.g., incipient wetness).[22,23] All of these methods have been investigated extensively as a means to improve surface area, porosity, microstructure, oxidation states, compositions, and catalyst stability. Despite remarkable progress, there remains a general demand for optimized synthetic methods to produce high surface area, sinter-resistant, multicomponent catalysts that are smoothly tailorable for the required catalytic application.

In addition, conventional catalyst preparation methods (especially wet-chemical synthesis) often entail multiple process steps that are time-consuming, difficult to control, and to some extent accompanied by the production of large amounts of useless waste. Flame aerosol synthesis and in particular liquid-feed flame spray pyrolysis (LF-FSP) offers an attractive alternative to traditional preparative techniques because it provides easy access to a wide variety of mixed-metal oxide solid solution and phase-separated nanopowders using one-step processing.[24−29] Flame aerosol synthesis is used widely to produce carbon-blacks, fumed silica, and titania pigments on a large scale with good cost-benefit ratios.[30] The flame-made metal-oxide nanopowders are usually characterized by high specific surface areas, nonporous structures, and improved resistance to sintering,[15] properties that appear to be very promising for multiple applications in heterogeneous catalysis.[29,31−37]

In LF-FSP processing, mixtures of metalloorganic precursors (metal carboxylates and/or alkoxides) dissolved in alcohol solvent are aerosolized with oxygen and afterward ignited via methane torches within a quartz chamber. Subsequent combustion of the aerosol at temperatures ranging from 1500 to 2000 °C followed by rapid quenching produces dispersible nanosized oxide powders with element ratios identical to those in the precursor solutions and occasionally with unknown phase compositions.[38,39] LF-FSP allows the production of up to five different oxide compositions within a single week and, therefore, may be regarded as a combinatorial method for synthesizing metal oxide powders.[24,40]

High-throughput experimentation (HTE) has recently emerged as valuable approach to discover new materials, especially catalysts, and is rapidly becoming a widely accepted tool in industrial as well as academic research.[41−53] In the field of heterogeneous catalysis, high-throughput approaches normally

(7) Machida, M.; Murata, Y.; Kishikawa, K.; Zhang, D.; Ikeue, K. *Chem. Mater.* **2008**, *20*, 4489–4494.
(8) Stark, W. J.; Maciejewski, M.; Mädler, L.; Pratsinis, S. E.; Baiker, A. *J. Catal.* **2003**, *220*, 35–43.
(9) Krishna, K.; Bueno-Lopez, A.; Makkee, M.; Moulijn, J. A. *Appl. Catal. B* **2007**, *75*, 189–200.
(10) Krishna, K.; Bueno-Lopez, A.; Makkee, M.; Moulijn, J. A. *Appl. Catal. B* **2007**, *75*, 201–209.
(11) Krishna, K.; Bueno-Lopez, A.; Makkee, M.; Moulijn, J. A. *Appl. Catal. B* **2007**, *75*, 210–220.
(12) Rao, G. R.; Kašpar, J.; Meriani, S.; Monte, R.; Graziani, M. *Catal. Lett.* **1994**, *24*, 107–112.
(13) Fornasiero, P.; Dimonte, R.; Rao, G. R.; Kaspar, J.; Meriani, S.; Trovarelli, A.; Graziani, M. *J. Catal.* **1995**, *151*, 168–177.
(14) Trovarelli, A. *Catalysis by Ceria and Related Materials*; Imperial College Press: London, 2002; Vol. 2.
(15) Schulz, H.; Stark, W. J.; Maciejewski, M.; Pratsinis, S. E.; Baiker, A. *J. Mater. Chem.* **2003**, *13*, 2979–2984.
(16) Di Monte, R.; Fornasiero, P.; Kapar, J.; Graziani, M.; Gatica, J. M.; Bernal, S.; Gómez-Herrero, A. *Chem. Commun.* **2000**, 2167–2168.
(17) Gobin, O. C.; Martinez Joaristi, A.; Schüth, F. *J. Catal.* **2007**, *252*, 205–214.
(18) Busch, O. M.; Hoffmann, C.; Johann, T. R. F.; Schmidt, H. W.; Strehlau, W.; Schuth, F. *J. Am. Chem. Soc.* **2002**, *124*, 13527–13532.
(19) Ozturk, S.; Senkan, S. *Appl. Catal. B* **2002**, *38*, 243–248.
(20) Richter, M.; Langpape, M.; Kolf, S.; Grubert, G.; Eckelt, R.; Radnik, J.; Schneider, M.; Pohl, M. M.; Fricke, R. *Appl. Catal. B* **2002**, *36*, 261–277.
(21) Krantz, K.; Ozturk, S.; Senkan, S. *Catal. Today* **2000**, *62*, 281–289.
(22) Delmon, B. *J. Therm. Anal. Calorim.* **2007**, *90*, 49–65.
(23) Ertl, G.; Knözinger, H.; Weitkamp, J. *Handbook of Heterogeneous Catalysis*; Wiley-VCH: Weinheim, Germany, 1997; Vol. 1.
(24) Kim, M.; Laine, R. M. *J. Ceram. Process. Res.* **2007**, *8*, 129–136.
(25) Sutorik, A. C.; Neo, S. S.; Treadwell, D. R.; Laine, R. M. *J. Am. Ceram. Soc.* **1998**, *81*, 1477–1486.
(26) Baranwal, R.; Villar, M. P.; Garcia, R.; Laine, R. M. *J. Am. Ceram. Soc.* **2001**, *84*, 951–961.
(27) Marchal, J.; John, T.; Baranwal, R.; Hinklin, T.; Laine, R. M. *Chem. Mater.* **2004**, *16*, 822–831.
(28) Kim, S.; Gislason, J. J.; Morton, R. W.; Pan, X. Q.; Sun, H. P.; Laine, R. M. *Chem. Mater.* **2004**, *16*, 2336–2343.
(29) Azurdia, J. A.; Marchal, J.; Shea, P.; Sun, H.; Pan, X. Q.; Laine, R. M. *Chem. Mater.* **2006**, *18*, 731–739.
(30) Oswald, M.; Deller, K. *Elements Degussa Science Newsletter* **2004**, *9*, 16–20.
(31) Piacentini, M.; Strobel, R.; Maciejewski, M.; Pratsinis, S. E.; Baiker, A. *J. Catal.* **2006**, *243*, 43–56.
(32) Strobel, R.; Krumeich, F.; Pratsinis, S. E.; Baiker, A. *J. Catal.* **2006**, *243*, 229–238.
(33) Strobel, R.; Krumeich, F.; Stark, W. J.; Pratsinis, S. E.; Baiker, A. *J. Catal.* **2004**, *222*, 307–314.
(34) Strobel, R.; Stark, W. J.; Mädler, L.; Pratsinis, S. E.; Baiker, A. *J. Catal.* **2003**, *213*, 296–304.
(35) Stark, W. J.; Wegner, K.; Pratsinis, S. E.; Baiker, A. *J. Catal.* **2001**, *197*, 182–191.
(36) Stark, W. J.; Pratsinis, S. E.; Baiker, A. *J. Catal.* **2001**, *203*, 516–524.
(37) Vormberg, R. *Elements Degussa Science Newsletter* **2004**, *9*, 21–23.
(38) Hinklin, T. R.; Azurdia, J.; Kim, M.; Marchal, J. C.; Kumar, S.; Laine, R. M. *Adv. Mater.* **2008**, *20*, 1373–1375.
(39) Laine, R. M.; Bickmore, C. R.; Treadwell, D. R.; Waldner, K. F. *J. Am. Ceram. Soc.* **1996**, *79*, 1419–1423.
(40) Azurdia, J.; Marchal, J.; Laine, R. M. *J. Am. Ceram. Soc.* **2006**, *89*, 2749–2756.
(41) Senkan, S. M.; Ozturk, S. *Angew. Chem., Int. Ed.* **1999**, *38*, 791–795.
(42) Bein, T. *Angew. Chem., Int. Ed.* **1999**, *38*, 323–326.
(43) Maier, W. F. *Angew. Chem., Int. Ed.* **1999**, *38*, 1216–1218.
(44) Jandeleit, B.; Schaefer, D. J.; Powers, T. S.; Turner, H. W.; Weinberg, W. H. *Angew. Chem., Int. Ed.* **1999**, *38*, 2494–2532.
(45) Hagemeyer, A.; Jandeleit, B.; Liu, Y.; Poojary, D. M.; Turner, H. W.; Volpe, A. F.; Henry Weinberg, W. *Appl. Catal. A* **2001**, *221*, 23–43.
(46) Senkan, S. *Angew. Chem., Int. Ed.* **2001**, *40*, 312–329.

consist of four closely connected elements: design of experiment, automated synthesis of catalyst libraries, high-throughput library screening, and data mining of the results. With reference to the automated catalyst synthesis, numerous different preparation methods have been successfully automated with the aid of robots. In addition to several sputtering techniques, the wet-chemical methods (e.g., precipitation,[54] impregnation,[55] and sol−gel preparation methods[56,57]) in particular have proved suitable for the high-throughput synthesis. Nevertheless, these approaches can turn into more complex tasks if multicomponent systems (e.g., quaternary catalyst composition spreads or supported multimetallic catalysts) have to be synthesized and varied in their compositions.[58] High-throughput screening methods also have another valuable advantage, all materials are studied under identical conditions, which allows direct comparison of the data.

Consequently, the first objective of the present investigation was to combine the unique features of LF-FSP for synthesis of multicomponent oxides with high-throughput technology (HTT) to accelerate the discovery of new lead catalyst compositions for the selective catalytic reduction of NO with propane as well as for the combustion of propane (propene).

Here we report results from the high-throughput screening of 46 different LF-FSP produced pure as well as mixed-metal oxide nanopowders by means of emissivity-corrected IR thermography (ecIRT).[59−62] A further objective of this work was to evaluate the general applicability of the presented flame-made materials for exhaust gas catalysis in comparison to commercial benchmark catalysts.

Experimental Section

A. Synthesis. 1. LF-FSP. The liquid-feed flame spray pyrolysis (LF-FSP) system has been described in detail elsewhere.[28,29,40] Ethanol precursor solutions were prepared by diluting the sample precursors to 2−5 wt % ceramic yield, typically 3 wt %. These solutions are then atomized with O_2 through a nozzle. The fine mist generated is ignited with methane/oxygen pilot torches, achieving combustion temperatures >1500 °C. The products are carried downstream by a radial pressure exhaust (19.8 m^3/min) and collected in electrostatic precipitators (ESPs) that are maintained at a 10 kV dc potential. The nanopowders are recovered manually from the ESP tubes after the apparatus has cooled down. Typical collection amounts for each of the 46 samples synthesized were 30−50 g. As stated earlier, one to three different compositions were produced per day due to the facile collection and large production rates per batch.

2. Powder Compacts. These were prepared by weighing ∼50 mg of powder and pressing it into a pellet (3.0 mm diameter) using a dual action hand press.

B. Analytical Methods. 1. Specific Surface Area Analyses (SSAs). SSAs were obtained using a Micromeritics ASAP 2010 sorption analyzer (Norcross, GA) for all nanopowders. Samples were loaded (350 mg) and degassed at 350 °C until a degas rate of <5 mTorr was achieved, followed by analysis at 77 K with N_2 as the adsorbate gas. The specific surface areas were calculated using the BET multipoint (10 points) method. The average particle diameter or size (APS) was determined by

$$\mathrm{APS_{BET}} = \frac{6}{\rho_{\mathrm{th}} \times \mathrm{SSA}} \quad (1)$$

where ρ_{th} is the theoretical density of the nanopowders, and SSA is the specific surface area.

For the reference catalysts (Hopcalite from Dräger Safety and 5 wt % Pt on Al_2O_3 from STREM Chemicals), nitrogen physisorption measurements were preformed on a Carlo Erba Sorptomatic 1990 at the temperature of liquid nitrogen (77 K). The samples were outgassed for 2 h under vacuum at 200 °C before adsorption. The specific surface areas were calculated using the BET multipoint method.

2. Scanning Electron Microscopy (SEM). Micrographs were taken using a Nova 600 Nanolab FIB/SEM (FEI Company, Hillsboro, OR). About 1 mg of nanopowder sample was first dispersed in 5 mL of DI water using an ultrasonic horn (Vibracell, Sonics and Materials Inc., Newton, CT) for 10 min. A drop of the dispersion was placed on a SEM sample stub, which was heated on a covered hot plate and the water allowed to evaporate. The stubs were then sputter coated with ∼180 Å of Au−Pd using a Technics Hummer VI sputtering system (Anatech, Ltd., Alexandria, VA) to improve resolution.

3. X-ray Diffraction Analyses (XRD). Analyses were performed on a Rigaku Miniflex (Rigaku, The Woodlands, TX). The diffractometer is equipped with a Cu X-ray tube (Cu $K\alpha_1$, λ = 1.54059 Å) with operating voltage of 30 kV and current of 15 mA. Scans were performed continuously from 20 to 80° 2θ in 0.03° increments at 2°/min. The nanopowder samples were prepared by packing ∼100 mg into an amorphous silica holder and loaded into the diffractometer. Scan data were analyzed using Jade 7.5 software (Materials Data, Inc., Livermore, CA) to determine average particle sizes (APSs) and phases present.

X-ray powder diffraction patterns for the reference catalysts (Hopcalite from Dräger Safety and 5 wt % Pt on Al_2O_3 from STREM Chemicals) were obtained using a Huber G670 Guinier image plate system with Cu $K\alpha_1$ radiation (λ = 1.54059 Å). For sample preparation, a few milligrams of powder was applied on adhesive tape in a sample holder. The data were accumulated continuously from 4 to 100° 2θ and analyzed using TOPAS software[63] to determine crystal data as lattice constants as well as average particle sizes ($\mathrm{APS_{XRD}}$) by Rietveld refinement.

4. Dynamic Light Scattering (DLS). DLS was also used to estimate APSs of LF-FSP nanopowders. Suspensions of each nanopowder in DI water (∼1 vol %) were loaded in compact goniometer system (ALV, Langen, Germany) equipped with a

(47) Mallouk, T. E.; Smotkin, E. S. Combinatorial Catalyst Development Methods. In *Handbook of Fuel Cells: Fundamentals, Technology and Applications*; Vielstich, W., Lamm, A., Gasteiner, H. A., Eds.; John Wiley & Sons: Chichester, UK, 2003; Vol. 2, pp 334−347.
(48) Bricker, M. L.; Sachtler, J. W. A.; Gillespie, R. D.; McGonegal, C. P.; Vega, H.; Bem, D. S.; Holmgren, J. S. *Appl. Surf. Sci.* **2004**, *223*, 109–117.
(49) Hendershot, R. J.; Snively, C. M.; Lauterbach, J. *Chem.—Eur. J.* **2005**, *11*, 806–814.
(50) Maier, W. F.; Stöwe, K.; Sieg, S. *Angew. Chem., Int. Ed.* **2007**, *46*, 6016–6067.
(51) Reetz, M. T. *Angew. Chem., Int. Ed.* **2001**, *40*, 284–310.
(52) Newsam, J. M.; Schüth, F. *Biotechnol. Bioeng.* **1998**, *61*, 203–216.
(53) Gennari, F.; Seneci, P.; Miertus, S. *Catal. Rev.* **2000**, *42*, 385–402.
(54) Hoffmann, C.; Wolf, A.; Schüth, F. *Angew. Chem., Int. Ed.* **1999**, *38*, 2800–2803.
(55) Rodemerck, U.; Wolf, D.; Buyevskaya, O. V.; Claus, P.; Senkan, S.; Baerns, M. *Chem. Eng. J.* **2001**, *82*, 3–11.
(56) Scheidtmann, J.; Weiss, P. A.; Maier, W. F. *Appl. Catal. A* **2001**, *222*, 79–89.
(57) Kim, D. K.; Maier, W. F. *J. Catal.* **2006**, *238*, 142–152.
(58) Hannemann, S.; Grunwaldt, J.-D.; Lienemann, P.; Günther, D.; Krumeich, F.; Pratsinis, S. E.; Baiker, A. *Appl. Catal. A* **2007**, *316*, 226–239.
(59) Holzwarth, A.; Schmidt, H.-W.; Maier, W. F. *Angew. Chem., Int. Ed.* **1998**, *37*, 2644–2647.
(60) Holzwarth, A.; Maier, W. F. *Platinum Met. Rev.* **2000**, *44*, 16–21.
(61) Kirsten, G.; Maier, W. F. *Appl. Surf. Sci.* **2004**, *223*, 87–101.
(62) Kirsten, G.; Maier, W. F. Relative Quantification of Catalytic Activity in Combinatorial Libraries by Emissivity-Corrected Infrared Thermography. In *High Throughput Screening in Chemical Catalysis*; Hagemeyer, A., Strasser, V., Volpe, A. F., Eds.; Wiley-VCH: Weinheim, Germany, 2004.
(63) *TOPAS*, version 2.1 (General profile and structure analysis software for powder diffraction data); Bruker AXS: Karlsruhe, Germany, 2000.

Table 1. Catalysts in Slate Library Plate

catalyst	short description	composition	source	count
MO (M = Ni)	M_x	$x = 100$	this work	3
MO_2 (M = Ce, Zr)	(M = Ce, Ni, Zr)			
$(CeO_2)_{x/100}(Al_2O_3)_{1-(x/100)}$	Ce_xAl_{100-x}	x = 0.10, 0.50, 1.00, 1.50, 2.00, 3.00, 5.00, 6.00, 7.50, 15.0, 30.0, 50.0, 75.0, 95.0	this work	14
$(CeO_2)_{x/100}(ZrO_2)_{1-(x/100)}$	Ce_xZr_{100-x}	x = 10.0, 30.0, 50.0, 70.0, 90.0	this work	5
$(CeO_2)_{x/100}(ZrO2)_{y/100}(Al_2O_3)_{1-((x+y)/100)}$	$Ce_xZr_yAl_{100-(x+y)}$	x = 35.0, 49.0, 63.0 y = 15.0, 21.0, 27.0	this work	3
$(CoO)_{x/100}(Al_2O_3)_{1-(x/100)}$	Co_xAl_{100-x}	x = 5.00, 10.0, 25.0, 70.0, 85.0	this work	5
$(NiO)_{x/100}(Al_2O_3)_{1-(x/100)}$	Ni_xAl_{100-x}	x = 5.00, 10.0, 22.0, 25.0, 50.0, 80.0	this work	6
$(NiO)_{x/100}(CuO)_{1-(x/100)}$	Ni_xCu_{100-x}	x = 50.0, 75.0	this work	2
$(ZrO_2)_{x/100}(Al_2O_3)_{1-(x/100)}$	Zr_xAl_{100-x}	x = 2.40, 4.10, 4.60, 5.90, 8.40, 13.6, 49.7, 80.6	this work	8
Pt/Al_2O_3 (reference)	Pt/Al_2O_3		Strem	1
Hopcalite (reference)	Hopcalite		Dräger Safety	1

multitau digital correlator (ALV-5000E, Langen, Germany). The laser source had a wavelength of $\lambda_0 = 0.488$ μm (Innova 70C, Coherent Inc., Santa Clara, CA).

C. Notation for Catalysts (Short Description). A simple notation was used to name the examined oxides, whereby, for example, a ternary oxide mixture is indicated by the contraction $A_xB_yC_{100-(x+y)}$ generally. The upper case A, B, and C stand for a particular metal oxide, the lower case x and y describe the share of the respective oxide in mol %.

D. High-Throughput Screening of Nanoparticle Catalysts. The catalyst pellets were crushed, and the resulting powders (see Table 1) were manually transferred into hexagonally positioned wells of a slate library plate (see Figure 1). Emissivity-corrected IR thermography (ecIRT) was used for the parallel detection of heat production on the surface of the catalyst beds, which is considered to be proportional to catalytic activity. The setup for parallel screening by means of ecIRT, as well as its measurement principles, has been described in detail elsewhere.[59−62] For the IR thermographic investigation, the library plate was inserted in a gastight, gas flow reactor with an IR transparent sapphire window on the top, allowing IR imaging of the library surface with an IR camera (PtSi crystal detector with 256 × 256 pixel, Thermosensorik Corp.). The whole experimental setup, including gas dosing, temperature, and IR camera control, was managed automatically with the IRTestRig software.[64]

Prior to the measurement, the library was pretreated at 380 °C for 30 min in synthetic air (50 mL/min) to evaporate water and oxidize volatile organic combustion residues (if present). After that, a six-point temperature calibration was carried out in a range of 10 K in the area of −4 to +6 K around each specific reaction temperature under nitrogen gas atmosphere. To examine the catalytic activity of the library samples (for propane oxidation and NO_x reduction), the reactor was held at 300 °C and five different reaction gas mixtures (see Table 2) passed successively through the system with a constant flow rate of 50 mL/min. The mixtures mainly varied in oxygen as well as NO_x content, contained nitrogen as carrier gas, and the reaction sequence started from the mixture with highest O_2 content (no. 1, Table 2).

Table 2. Compositions of Reaction Gas Mixtures

mixture no.	brief description	$c(C_3H_8)$ [vol %]	$c(NO)$ [vol %]	$c(O_2)$ [vol %]	$c(N_2)$ [vol %]
1	C_3H_8 20.0% O_2	0.40	0.00	20.0	79.6
2	C_3H_8 NO 20.0% O_2	0.40	0.20	20.0	79.4
3	C_3H_8 NO 5.00% O_2	0.40	0.20	5.00	94.4
4	C_3H_8 NO 1.00% O_2	0.40	0.20	1.00	98.4
5	C_3H_8 NO	0.40	0.20	0.00	99.4

A series of four IR images were recorded at certain times for each reaction gas atmosphere, after 1, 5, 10, and 30 min of reaction time as test on steady-state conditions. The images after 30 min were always used later to evaluate the relative catalytic activities. Each series of images was followed by the recording of a background image at the reaction temperature under inert nitrogen gas atmosphere for the subsequent emissivity correction.

E. Conventional Screening Experiments. Samples of 6 m^2/g of $Ce_{0.5}Zr_{0.5}O_2$ and 20 m^2/g $Ce_{0.7}Zr_{0.3}O_2$ nanopowders were tested for catalytic activity toward NO_x reduction and propene oxidation in a conventional gas-phase flow reactor. Thus, 0.070 g of the oxide was loaded into a quartz U-tube flow reactor (i.d. 3.5 mm) and subjected to an inlet gas composition of 688 ppm NO, 20 ppm NO_2, 711 ppm propene, 10 vol % O_2, 2.5−3.0 vol % H_2O, and the remainder He. The total gas flow rate was 74 mL/min. The reactor was heated to selected temperatures, and the amounts of conversion were obtained at steady state at each temperature (i.e., the sample was kept under this inlet condition at a given temperature until the outlet concentration of NO and NO_2 were constant). Product analysis was performed using an online Mattson Galaxy Series FTIR (to determine N_2O, CO, and CO_2 concentration) and a Thermo Environmental 42CHL NO_x chemoluminescence analyzer (to measure NO and NO_2 concentration).

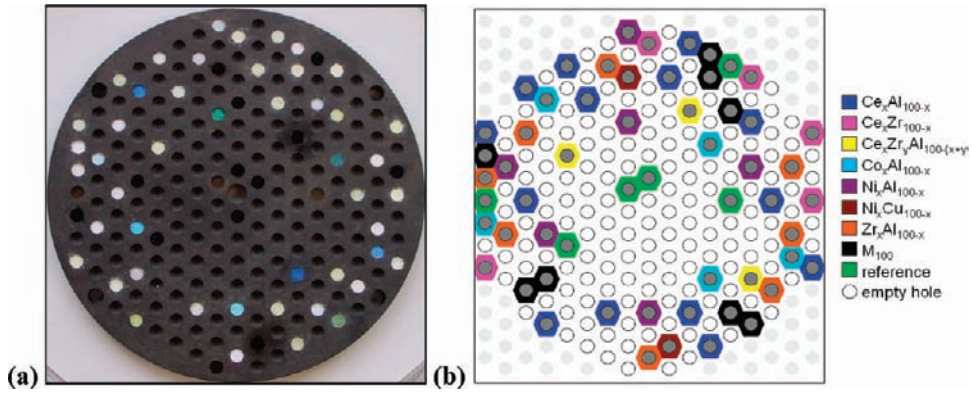

Figure 1. Images of (a) a slate library plate filled with 48 different catalyst powders and (b) layout of the library plate.

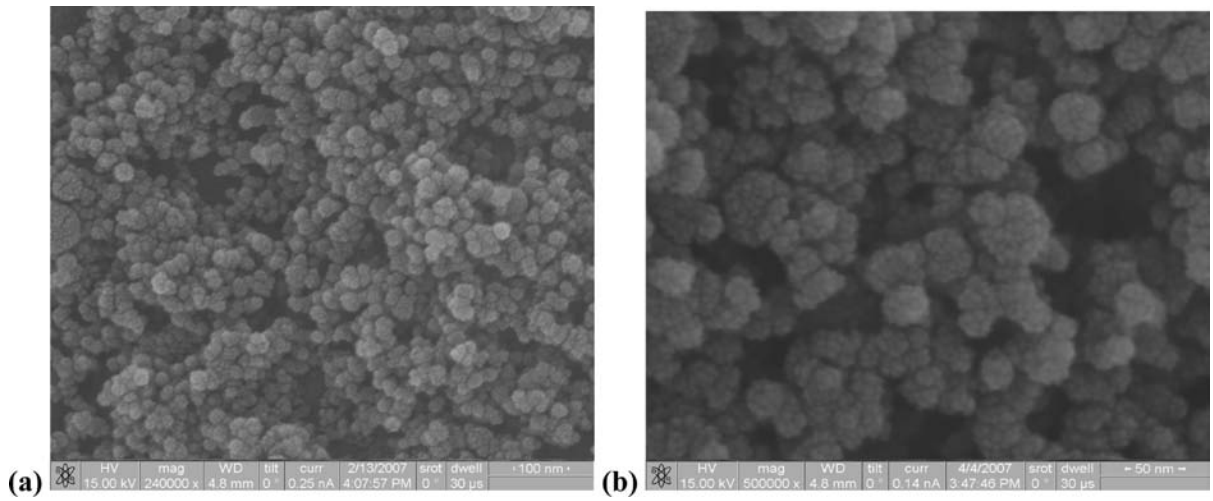

Figure 2. SEMs of (a) $(CeO_x)_{0.5}(Al_2O_3)_{0.5}$ and (b) $(CeO_x)_{0.1}(Al_2O_3)_{0.9}$.

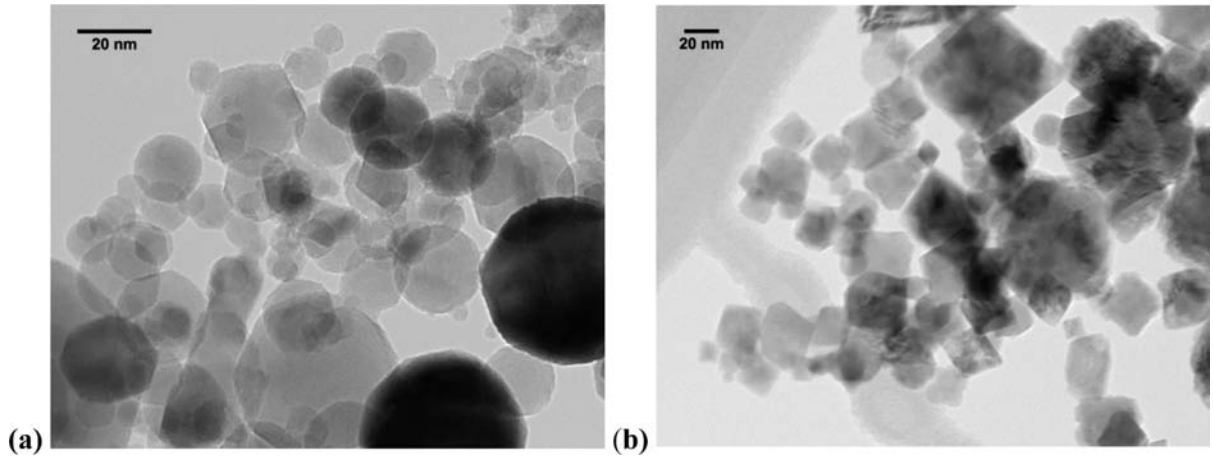

Figure 3. TEMs of (a) $(CoO_x)_{0.08}(Al_2O_3)_{0.92}$ and (b) $(CoO_x)_{0.80}(Al_2O_3)_{0.20}$ samples. Note change in particle morphology.

1. Pt Impregnation. Pt (0.5 wt %) was deposited onto the surface of 20 m^2/g of $Ce_{0.7}Zr_{0.3}O_2$ using standard methods described elsewhere.[65−67] The material was calcined at 500 °C for 5 h and then reduced with H_2 at 450 °C for 2 h.

Results and Discussion

In the following sections, we first provide some characterization data for selected catalyst powders that were used to produce the powder compacts used in the HTE studies. Thereafter, we discuss HTE studies and identify some of the more unusual results of these studies.

A. Catalyst Characterization. A variety of LF-FSP powders have been made and discussed in the literature.[24,29,38−40] Below we provide some selected examples of powder characterization to provide the basis for selected comments to be made in the HTE studies.

SEM was used to demonstrate powder uniformity. Figure 2 shows samples of $(CeO_x)_{0.5}(Al_2O_3)_{0.5}$ and $(CeO_x)_{0.1}(Al_2O_3)_{0.9}$, demonstrating that SEM resolution is insufficient to reveal individual particles but does provide a view of the general particle population. These SEMs indicate that the particle populations produced here do not include any obvious micrometer size particles.

TEM images were used to assess particle morphologies and sizes of as-prepared powders. Discussions of actual size/size distributions are not appropriate if based solely on TEM micrographs, unless combined with XRD line broadening results and/or specific surface area measurements.

In Figure 3, most of the particles are spherical and well below 80 nm in diameter, with the vast majority <30 nm. Note the change in morphology, which is mostly faceted and spherical for the $(CoO_x)_{0.08}(Al_2O_3)_{0.92}$ sample (Figure 3a), while nearly all particles in the $(CoO_x)_{0.80}(Al_2O_3)_{0.20}$ sample in Figure 3b appear rhombic. This is attributed to the formation of the highly crystalline spinel phase coincident with increases in Co content. Particle necks, while occasionally visible in the 8 mol % sample, are not a major morphological feature.

Figure 4 images are high-resolution TEM micrographs of $(ZrO_2)_x(Al_2O_3)_{1-x}$ nanopowders. The particle sizes here are typically <30 nm in diameter with most <20 nm. Figure 4b shows clearly visible lattice planes indicating a high degree of crystallinity. The lattice planes in a single particle are unidirectional, suggesting single crystal particles formed during rapid quench from the gas phase.

(64) Scheidtmann, J. Ph.D. Thesis, Universität des Saarlandes, Saarbrücken, 2003.
(65) Seker, E.; Cavataio, J.; Gulari, E.; Lorpongpaiboon, P.; Osuwan, S. *Appl. Catal. A* **1999**, *183*, 121–134.
(66) Seker, E.; Gulari, E. *Appl. Catal. A* **2002**, *232*, 203–217.
(67) Seker, E.; Yasyerli, N.; Gulari, E.; Lambert, C.; Hammerle, R. H. *Appl. Catal. B* **2002**, *37*, 27–35.

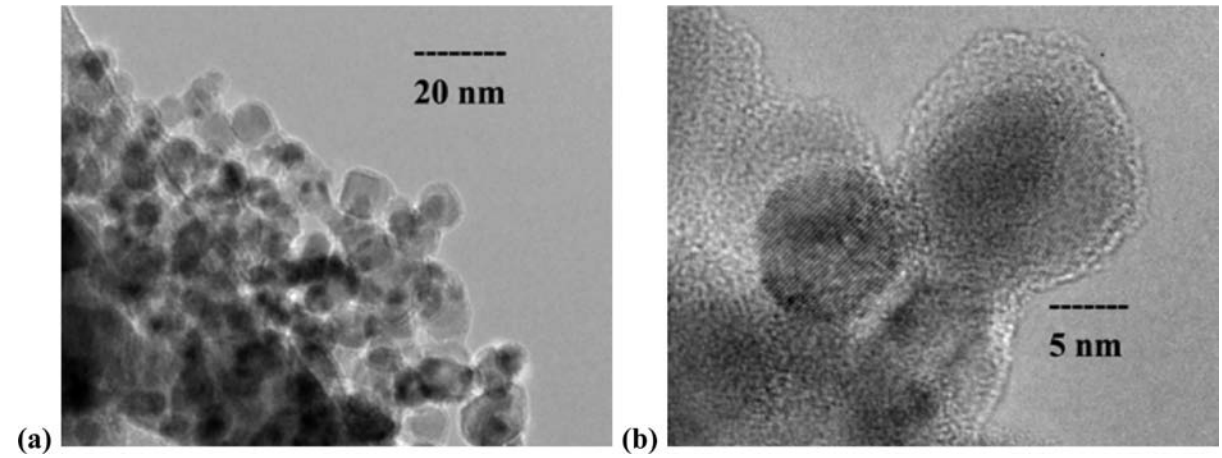

Figure 4. (a) TEM and (b) HR-TEM images of $(ZrO_x)_{0.80}(Al_2O_3)_{0.20}$.

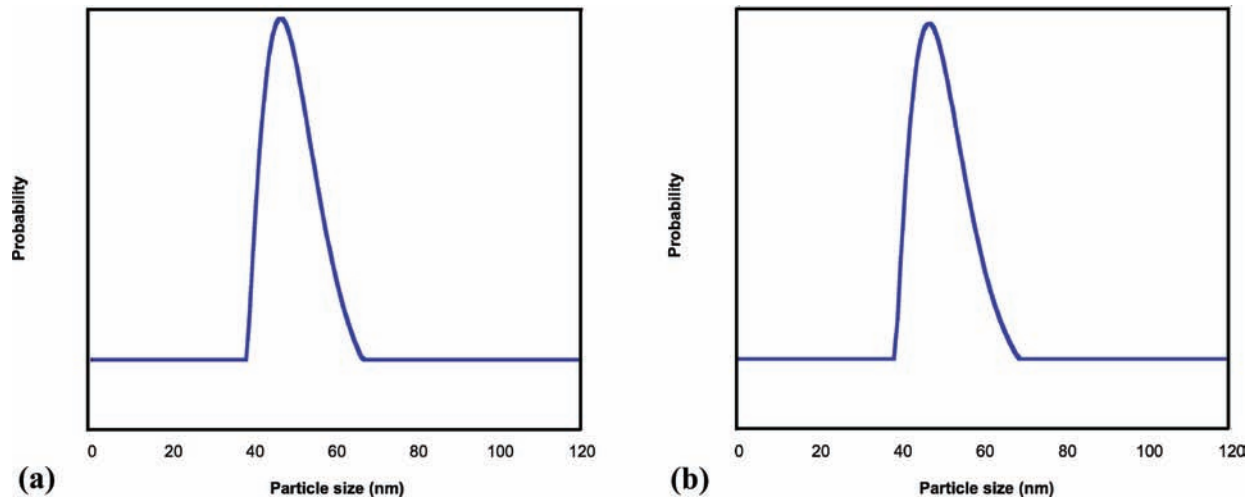

Figure 5. Particle size distribution of (a) $(ZrO_2)_{0.54}(Al_2O_3)_{0.46}$ and (b) $(CeO_x)_{0.50}(Al_2O_3)_{0.50}$ by dynamic light scattering.

Besides XRD and high-resolution microscopes, dynamic light scattering (DLS) was used to estimate average particle sizes (APSs). According to Figure 5, the APSs from DLS are about 20 nm higher than previous XRD results. These results suggest that we are measuring the hydrodynamic radius of the water layer on the nanoparticles in the DLS experiments.

The catalytic activity of an oxide is usually related to its textural properties, in particular, to its specific surface area. Therefore, in addition to particle size analyses based on DLS and X-ray line broadening, the specific surface area of selected catalysts was determined by BET methods to corroborate APSs. The results are reported in Table 3. The catalysts are listed according to their chemical compositions in order to allow a direct comparison between different classes of mixed oxides. The materials have surface areas ranging from 26 to 66 $m^2\ g^{-1}$. In some groups, the increase or decrease in surface area correlates with the changing content of one mixture component (e.g., Co_xAl_{100-x}), whereas in other cases, the surface area is not affected by this parameter.

Note that, due to the very small particle sizes of these flame made materials, they are completely nonporous but have a tendency to agglomerate (see Figure 2); otherwise, they are easily dispersed.[38] These characteristics have essential consequences for the catalytic properties of these materials because the kinetics of a heterogeneously catalyzed reaction are generally influenced by mass transport processes. In connection with this, one distinguishes between the external mass diffusion (film diffusion) and the internal mass diffusion (pore diffusion) of reactants or products. The latter should not affect the reaction rate of the examined nanocatalysts since they are not porous. On the other hand, the agglomeration of the particles forms voids within the agglomerates, which represent diffusion barriers similar to micro- and mesopores. In view of this, a direct comparison between the catalytic performances of the examined mixed-metal oxide nanopowders and the used benchmark materials (Pt on Al_2O_3 and Hopcalite) appears only conditionally favorable since their physical properties (porosity, surface area) are fundamentally different. Particularly, the much higher surface areas of the two reference materials should be taken into account when they are ranked according to their activity against the nanopowders. Furthermore, the degree of Pt metal dispersion in the commercial catalysts is not known sufficiently accurately to allow a direct comparison of catalyst activities.

B. High-Throughput Experiments. 1. Discussion. The application of high-throughput and combinatorial techniques in the development of new materials allows one to significantly enhance the number of experiments carried out during a given time. In contrast to conventional one-at-a-time approaches, high-throughput research methods make use of materials libraries containing numerous different components which are synthesized and tested for the desired application in a highly parallel or fast sequential manner with a high degree of automation and

Table 3. Main Physical and Structural Properties of Selected Catalyst Powders

catalyst	short description	SSA_{BET} [$m^2\ g^{-1}$] ± 5%	APS_{BET} [nm] ± 5%	APS_{XRD} [nm] ± 5%	structure
Al_2O_3	Al_{100}	66	29	29	
CeO_2	Ce_{100}	45	20	20	cubic
$(CeO_2)_{0.05}(Al_2O_3)_{0.95}$	$Ce_{5.00}Al_{95.0}$	60	24	14	magnetoplumbite
$(CeO_2)_{0.075}(Al_2O_3)_{0.935}$	$Ce_{7.50}Al_{92.5}$	63	22	17	cubic
$(CeO_2)_{0.10}$ $(Al_2O_3)_{0.90}$	$Ce_{10.0}Al_{90.0}$	57	22	14	cubic
$(CeO_2)_{0.15}(Al_2O_3)_{0.85}$	$Ce_{15.0}Al_{85.0}$	60	20	15	cubic
$(CeO_2)_{0.30}(Al_2O_3)_{0.70}$	$Ce_{30.0}Al_{70.0}$	57	20	15	cubic
$(CeO_2)_{0.50}(Al_2O_3)_{0.50}$	$Ce_{50.0}Al_{50.0}$	50	20	16	cubic
$(CeO_2)_{0.75}(Al_2O_3)_{0.25}$	$Ce_{75.0}Al_{25.0}$	45	20	18	cubic
$(CeO_2)_{0.95}(Al_2O_3)_{0.05}$	$Ce_{95.0}Al_{5.00}$	45	20	20	cubic
$(CeO_2)_{0.1}(ZrO_2)_{0.9}$	$Ce_{10.0}Zr_{90.0}$	32	28	16	tetragonal
$(CeO_2)_{0.3}(ZrO_2)_{0.7}$	$Ce_{30.0}Zr_{70.0}$	32	28	16	tetragonal/cubic
$(CeO_2)_{0.5}(ZrO_2)_{0.5}$	$Ce_{50.0}Zr_{50.0}$	32	28	16	cubic
$(CeO_2)_{0.7}(ZrO_2)_{0.3}$	$Ce_{70.0}Zr_{30.0}$	33	26	16	cubic
$(CeO_2)_{0.9}(ZrO_2)_{0.1}$	$Ce_{90.0}Zr_{10.0}$	36	22	16	cubic
$(CeO_2)_{0.49}(ZrO_2)_{0.21}(Al_2O_3)_{0.3}$	$Ce_{49.0}Zr_{21.0}Al_{30.0}$	45	22	13	cubic
$(CeO_2)_{0.63}(ZrO_2)_{0.27}(Al_2O_3)_{0.1}$	$Ce_{63.0}Zr_{27.0}Al_{10.0}$	42	20	16	
$(CoO)_{0.04}(Al_2O_3)_{0.96}$	$Co_{4.00}Al_{96.0}$	53	31	18	
$(CoO)_{0.08}(Al_2O_3)_{0.92}$	$Co_{8.00}Al_{92.0}$	53	30	21	
$(CoO)_{0.21}(Al_2O_3)_{0.79}$	$Co_{21.0}Al_{79.0}$	51	30	20	
$(CoO)_{0.50}(Al_2O_3)_{0.50}$	$Co_{50.0}Al_{50.0}$	38	38	22	
$(CoO)_{0.87}(Al_2O_3)_{0.13}$	$Co_{87.0}Al_{13.0}$	30	35	21	
$(CoO)_{0.94}(Al_2O_3)_{0.06}$	$Co_{94.0}Al_{6.00}$	26	40	22	
$(NiO)_{0.43}(Al_2O_3)_{0.57}$	$Ni_{43.0}Al_{57.0}$	69	18	20	spinel
$(NiO)_{0.63}(Al_2O_3)_{0.47}$	$Ni_{63.0}Al_{47.0}$	58	19	22	spinel
$(NiO)_{0.78}(Al_2O_3)_{0.22}$	$Ni_{78.0}Al_{22.0}$	45	23	20	NiO/spinel
$(ZrO_2)_{0.024}(Al_2O_3)_{0.976}$	$Zr_{2.40}Al_{97.6}$	54	28	14	delta
$(ZrO_2)_{0.041}(Al_2O_3)_{0.959}$	$Zr_{4.10}Al_{95.9}$	57	26	18	delta
$(ZrO_2)_{0.059}(Al_2O_3)_{0.941}$	$Zr_{5.90}Al_{94.1}$	57	26	15	delta
$(ZrO_2)_{0.136}(Al_2O_3)_{0.864}$	$Zr_{13.6}Al_{86.4}$	47	30	13	tetragonal/ delta
$(ZrO_2)_{0.497}(Al_2O_3)_{0.503}$	$Zr_{49.7}Al_{50.3}$	53	22	12	tetragonal/ delta
$(ZrO_2)_{0.794}(Al_2O_3)_{0.206}$	$Zr_{79.4}Al_{20.6}$	51	22	12	tetragonal/ delta
Pt/Al_2O_3 (reference)	Pt/Al_2O_3	103			nearly amorphous
Hopcalite (reference)	Hopcalite	174			amorphous

miniaturization.[50] Hence, these methods provide a perfect tool to accelerate the discovery and optimization of new heterogeneous catalysts. However, in order to seek out new and, in particular, formally unknown lead catalyst compositions, a nearly infinite chemical parameter space has to be explored. Even with high-throughput methods, it is impossible to systematically search through such a huge space. Therefore, HTE has to be combined with suitable discovery and/or optimization strategies in order to effectively search for new catalysts in a reasonable time-to-benefit ratio.[61]

A high-throughput study often starts with an initial screening of several highly diverse starting libraries with the intention to cover the selected parameter space. The results of these experiments (identification of active materials) provide the basis for the selection of promising materials for the next generations of libraries with reference to the chosen development strategy. The synthesis of these libraries normally comprises a compositional variation and/or an additional doping with different elements to obtain further improvements of the catalytic activity.

The results presented in this work are considered as part of a prescreening sequence of different binary and ternary flame-made metal oxides with the main intention to evaluate the general applicability of these materials for the selective catalytic reduction of NO with propane (propene) as well as for propane (propene) combustion in comparison to commercial benchmark catalysts. As already described in the prior section, all examined oxides were prepared by LF-FSP with an average production rate of up to 10 materials per week. Compared to other well-proven high-throughput synthesis techniques,[54−57] this seems to be a major bottleneck in our approach. Nevertheless, in the light of the numerous exclusive advantages provided by LF-FSP (e.g., one-step preparation of multicomponent nanosized mixed-metal oxides), this restriction appears to be just a small hindrance, which can easily be overcome by a supplementary automation and parallelization of the method. Consequently, this study is regarded as an initial step for further investigations in this field.

The prepared metal oxides as well as the commercially available references (see Table 1) were used to generate a starting library of 48 materials. Emissivity-corrected infrared thermography (ecIRT) was used for the rapid parallel screening of the library to monitor the heat production on the surface of the materials under different reaction gas atmospheres, followed by quantification of the individual heat spots with appropriate software.

In general, the exposure of a catalyst surface to a reaction gas mixture leads either to heat production, if exothermic reactions take place, or to heat consumption due to endothermic reactions. The total sum of heat emitted is proportional to the linear combination of catalytic activity and the enthalpies of all occurring reactions.[62] Therefore, the visualization of reaction heats by means of ecIRT provides no detailed information about the selectivity of the analyzed catalysts. This is a critical fact particularly for reactions with parallel and sequential side reactions because the recorded heat increase may be generated not only by higher catalytic activity but also by an increase in side reactions. The measurement conditions chosen in this study (see Experimental Section) enable several possible reaction pathways for propane and NO (see eqs 2−9 in Table 4). The desired selective reduction of NO with propane to N_2 (eq 5)

Table 4. Chemical Equations and Calculated Reaction Enthalpies[68,69]

chemical equation	$\Delta_R H^0_{298}$ [kJ/mol]
$C_3H_8(g) + 5O_2(g) \rightarrow 3CO_2(g) + 4H_2O(g)$ (2)	−2219.9
$C_3H_8(g) + {}^7/_2O_2(g) \rightarrow CO_2(g) + CO(g) + C(s) + 4H_2O(g)$ (3)	−1372.1
$NO(g) + {}^1/_2O_2(g) \rightleftharpoons NO_2(g)$ (4)	−57.2
$4NO(g) + C_3H_8(g) + 3O_2(g) \rightarrow 2N_2(g) + 3CO_2(g) + 4H_2O(g)$ (5)	−2581.1
$10NO(g) + C_3H_8(g) \rightarrow 5N_2(g) + 3CO_2(g) + 4H_2O(g)$ (6)	−3122.9
$2NO(g) + C_3H_8(g) + {}^9/_2O_2(g) \rightarrow N_2O(g) + 3CO_2(g) + 4H_2O(g)$ (7)	−2318.5
$C_3H_8(g) \rightarrow C_3H_6(g) + H_2(g)$ (8)	+124.2
$NO(g) \rightarrow {}^1/_2N_2(g) + {}^1/_2O_2(g)$ (9)	−90.3

and nearly all other reactions (with the exception of reaction 8) are exothermic and might occur either alone or simultaneously and hence are recorded altogether during the ecIRT measurement.

According to literature, the mechanisms for selective catalytic reduction of NO_x by hydrocarbons can be divided into two classes. The so-called "adsorption/dissociation mechanism" is regarded as applicable to describe reactions on noble metal and Cu-ZSM5 catalysts.[4,70,71] This mechanism involves adsorption of NO on active metal sites, which then dissociates into N(ads) and O(ads). Thereafter, combination of two N(ads) produces N_2, whereas O(ads) reacts with hydrocarbons to form CO_2. Remaining undissociated NO reacts with N(ads) to form N_2O.

The second, "oxidation−reduction mechanism" seems to be suitable for metal-oxide catalysts.[4,72] According to this mechanism (for illustration see literature reference), NO reacts first with adsorbed oxygen to form reactive intermediates like NO_2 or NO_3(ads). Simultaneously, the hydrocarbon is oxidized at the catalyst surface to hydrocarbon oxygenates (e.g., acetate). These oxygenates undergo further reactions with surface nitrates to produce organo-nitrogen species, which hydrolyze to form NH_3, R-NCO, or R-CN (g or ads). The hydrolyzed intermediates react with NO_2/NO or surface nitrates to produce N_2. Accordingly, the adsorbed oxygen appears in this mechanism as an activator for NO as well as for hydrocarbons and furthermore the remaining gas-phase oxygen is able to oxidize NO to more reactive NO_2. NO_2 is also proven to have an important function for the whole process because it rapidly reacts with some other key intermediates such as R-CN to form N_2.

Apart from oxygen's beneficial properties, it also has an undesired effect. At higher temperatures, the unselective combustion of hydrocarbons becomes much faster than selective catalytic reduction of NO. Therefore, the conversion of NO_x starts to decrease as the temperature increases.

Independent of the true reaction mechanism, the adsorption of NO and hydrocarbon combined with their activation on catalytic sites has a significant influence on reaction initiation. Furthermore, the relevance and rate of each mechanistic step depends strongly on the nature of the active site(s) and the experimental conditions. Note that both mechanisms were postulated to occur based on studies using unsaturated hydrocarbons (e.g., propene) as reducing agent and are therefore just conditionally applicable to the results discussed below. More specifically, already in 1997 Burch et al.[73] pointed out that there is a remarkable difference between alkanes and alkenes in the reduction of NO by hydrocarbons over Pt catalysts under lean-burn conditions.

However, the two proposed mechanisms at least allow classification of the reactions in Table 4 into promotional or obstructive side reactions with regard to propane-SCR. Obviously, the pure combustion of propane to CO_2 and water (eq 2) as well as the conversion of NO to N_2O (eq 7) must be considered as undesired side reactions because both are strongly exothermic and therefore give misleading activity results in the ecIRT screening. As already mentioned, at higher temperatures, propane combustion is the favored reaction, whereas the conversion of NO to N_2O decreases with rising temperature after going through a maximum (in particular over noble metal catalysts).[73]

A complete suppression of these side reactions by modifying the reaction conditions (oxygen exclusion from feed gas, decrease of reaction temperature) is not possible because the desired test reaction (eq 5) requires a specific and exclusive reaction path in the energy hyper-surface. However, the probability of finding this situation without additional local minima for catalysts is very low. Also, the influence on parameters (e.g., temperature) is limited because very low heat emissions are difficult to record by ecIRT. Consequently, the results reported here allow no general conclusions about the catalytic selectivity of a particular active sample. These initial studies are useful both for excluding inactive materials and for identifying new catalyst systems not expected based on the literature and therefore represent successful discoveries of new points of departure for further studies.

2. Results. For the high-throughput screening, a reaction temperature of 300 °C was chosen and the oxygen content of the feed gas was varied between 0 and 20 vol %. This intentional variation was used to discover materials that exhibit heat production (catalytic activity) at low oxygen concentrations. Furthermore, in one part of the applied screening program, NO was omitted from the feed gas to explore the catalytic activity

(68) Binnewies, M.; Milke, E., *Thermochemical Data of Elements and Compounds*, 2nd ed.; Wiley-VCH: Weinheim, Germany, 1999.
(69) Barin, I.; Knacke, O.; Kubaschewski, O., *Thermochemical Properties of Inorganic Substances*; Springer-Verlag: Berlin, 1977.
(70) Burch, R.; Millington, P. J.; Walker, A. P. *Appl. Catal. B* **1994**, *4*, 65–94.
(71) Walker, A. P. *Catal. Today* **1995**, *26*, 107–128.
(72) Meunier, F. C.; Zuzaniuk, V.; Breen, J. P.; Olsson, M.; Ross, J. R. H. *Catal. Today* **2000**, *59*, 287–304.
(73) Burch, R.; Watling, T. C. *Catal. Lett.* **1997**, *43*, 19–23.

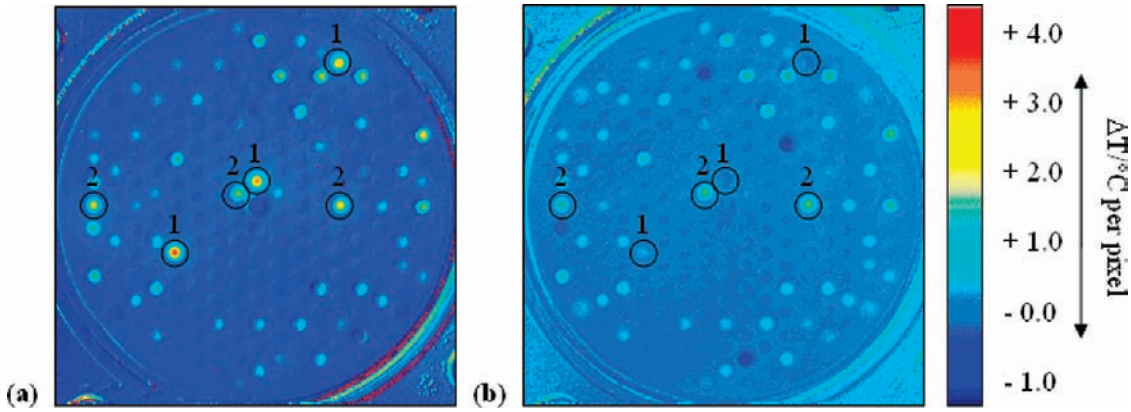

Figure 6. Emissivity-corrected IR thermographic images of catalyst library after 30 min under reaction gas atmosphere containing 20 vol % O_2, 0.4 vol % propane, 0.2 vol % NO, and N_2 as balance at 300 °C (a) or 0.4 vol % propane, 0.2 vol % NO, and N_2 as balance at 300 °C (b). 1: Hopcalite; 2: 5 wt % Pt on Al_2O_3.

of all library samples for pure combustion of propane. Prior to the measurement, the library was pretreated at 380 °C for 30 min in a flow of synthetic air for 30 min to clean the catalysts' surfaces from water and organic combustion residues (if present).

Note that the following discussion of the high-throughput screening results is based on a ranking of the different examined catalysts according to their heat production on the surface under reaction conditions, which is considered to be proportional to catalytic activity. In this context, the concept of catalytic activity is therefore not used in terms of a specific rate of reaction because it is not possible to record specific reaction rates by means of ecIRT. The identification of a certain catalyst as highly active has to be understood in terms of a higher heat emission of this material in comparison to all other library components.

Figure 6 shows two emissivity-corrected IR thermographic images of the examined library under oxygen-rich as well as under oxygen poor-reaction conditions. The yellow to red colored dots in the images mark materials that show heat production after exposing the library for 30 min to a selected reaction gas mixture at 300 °C. In general, the appearance of numerous heat spots beside the expected ones from the commercial benchmarks (Hopcalite and Pt on Al_2O_3) indicates a potential capability of the analyzed flame-made mixed oxides for catalytic oxidation.

From a simple comparison of the two images, it becomes obvious that all samples demonstrate higher heat emission under oxygen-containing reaction conditions. This result is not really surprising but confirms the already discussed crucial role of oxygen to function as an activator for several chemical processes.

One of the most notable findings is the high activity of the reference Hopcalite under oxygen excess, whereas the same catalyst becomes nearly inactive when oxygen is excluded from the feed gas. This result is in good agreement with literature since Hopcalite, a mixture of copper(II) and manganese(IV) oxides, is well-known for its high catalytic activity in low-temperature oxidation of CO to CO_2[74] and in the catalytic combustion of volatile organic compounds (VOC).[75,76] Carbon monoxide is not present in the initially injected reaction gas mixture. This fact suggests that the visualized heat production over this catalyst is primarily induced by the combustion of propane, which is inhibited when oxygen is excluded from the feed gas.

The second reference Pt supported on Al_2O_3 is characterized by a lower heat emission under oxygen-rich conditions compared to Hopcalite, but in contrast, it seems to retain some activity when oxygen is excluded from the feed gas. It is long proven that this noble metal catalyst has a certain activity for the reduction of NO to N_2 with hydrocarbons in the presence of excess oxygen (eq 5).[70] On the other hand, this catalyst is also characterized by a comparatively poor selectivity toward N_2 (due to the formation of N_2O) and a narrow activity temperature window.[2] The recorded heat emission over this reference is therefore attributed to several parallel reactions. It is obvious that under excess oxygen, reactions 2, 5, and 7 of Table 4 are the primary contributors to the total heat. Which of these reactions take place preferentially under the selected conditions is not derivable from the measurement results.

The fact that this catalyst additionally shows slight heat emission in the absence of oxygen suggests a potential catalytic activity for reactions involving just propane and/or NO. Possible reaction pathways that have to be mentioned in this relationship are the dehydrogenation of propane (eq 8), the direct conversion of propane with NO (eq 6), and the decomposition of NO (eq 9). Pt and, in particular, Pt−Sn supported on alumina are used widely in industry as catalyst for the selective dehydrogenation of propane to propene.[77,78] Since this is an endothermic reaction, which requires relatively high temperatures (ca. 500−600 °C), even in the presence of a catalyst, it cannot proceed under the conditions used here.

Furthermore, a reaction between NO and propane without oxygen as an additional reaction partner (eq 6) seems to be kinetically unfavorable because propane (as saturated hydrocarbon) is comparatively chemically inert, and a large excess of NO is required to convert 1 equiv of propane to CO_2 and H_2O. The decomposition of NO into N_2 and O_2 is slightly exothermic and known to be catalyzed by La_2O_3-, Ba/MgO-, and $LaCoO_3$-based perovskite oxides.[79] However, this reaction proceeds, like propane dehydrogenation, only at high temperatures (ca. 800 °C) and therefore cannot be responsible for the recorded heat emission.

(74) Lamb, A. B.; Bray, W. C.; Frazer, J. C. W. *J. Ind. Eng. Chem.* **1920**, *12*, 213–221.
(75) Lintz, H. G.; Wittstock, K. *Appl. Catal. A* **2001**, *216*, 217–225.
(76) Musick, J. K.; Williams, F. W. *Product R&D* **1975**, *14*, 284–286.
(77) Kogan, S. B.; Schramm, H.; Herskowitz, M. *Appl. Catal. A* **2001**, *208*, 185–191.
(78) Yu, C.; Ge, Q.; Xu, H.; Li, W. *Catal. Lett.* **2006**, *112*, 197–201.
(79) Ishihara, T.; Ando, M.; Sada, K.; Takiishi, K.; Yamada, K.; Nishiguchi, H.; Takita, Y. *J. Catal.* **2003**, *220*, 104–114.

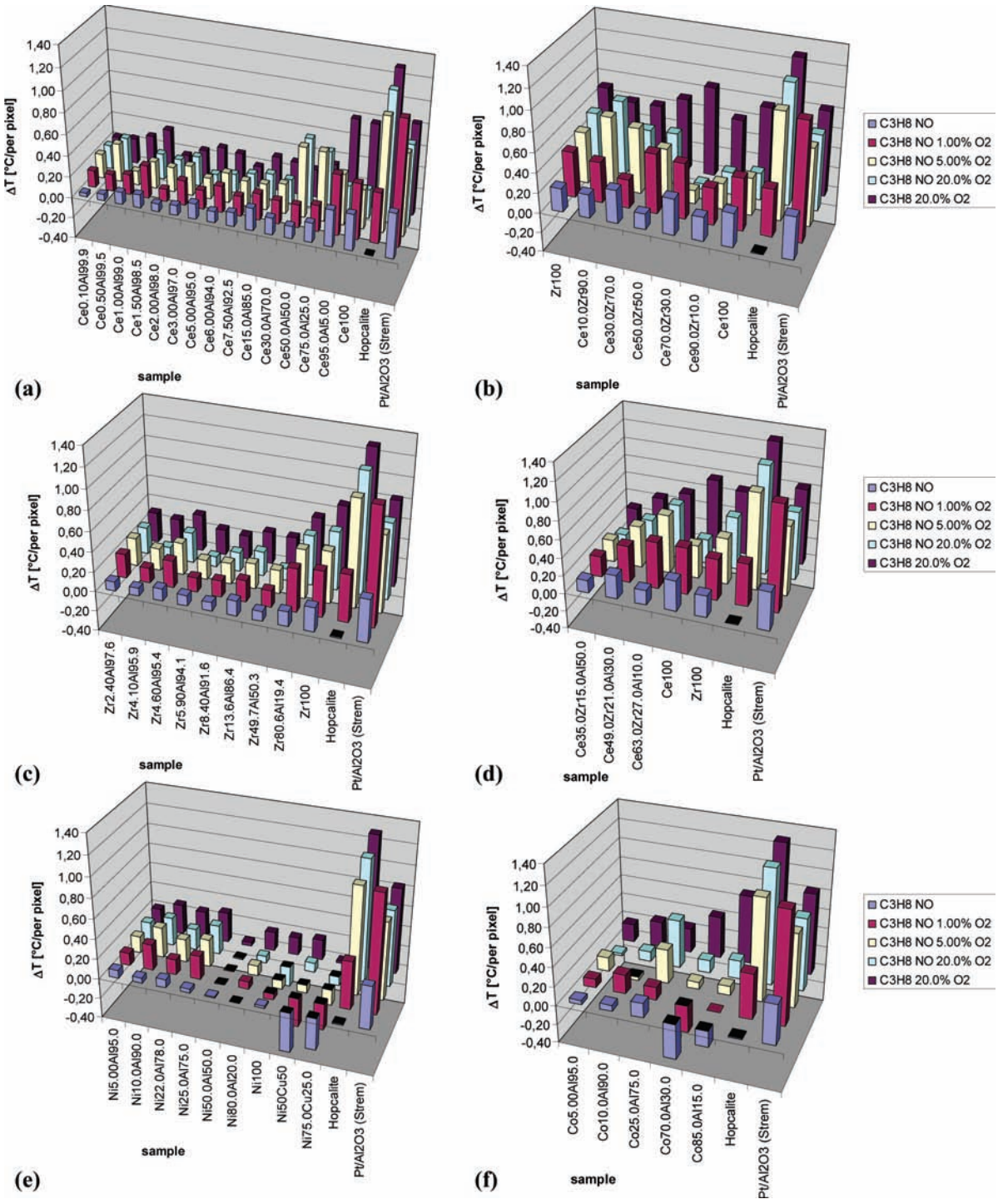

Figure 7. Emissivity-corrected IR thermography screening results for seven groups of nanoparticle catalysts under five different reaction gas atmospheres. Ce_xAl_{100-x} (a), Ce_xZr_{100-x} (b), Zr_xAl_{100-x} (c), $Ce_xZr_yAl_{100-(x+y)}$ (d), $Ni_xAl_{100-x}/Ni_xCu_{100-x}$ (e), and Co_xAl_{100-x} (f).

The most reasonable explanation for the apparent warming under oxygen exclusion is presumably due to emissivity changes and not by any type of catalytic reaction. Only in the case of Pt on Al_2O_3 a certain degree of NO reduction cannot be ruled out. This conclusion is valid in the same way for all other catalysts that exhibit heat emission under oxygen exclusion.

With reference to chemical composition, the different library samples are classified as follows: (I) Ce_xAl_{100-x}, (II) Ce_xZr_{100-x}, (III) Zr_xAl_{100-x}, (IV) $Ce_xZr_yAl_{100-x}$, (V) Co_xAl_{100-x}, (VI) Ni_xAl_{100-x}, and (VII) Ni_xCu_{100-x}. The recorded temperature changes for every sample within these seven groups are illustrated by bar diagrams in Figure 7. Most of the materials exhibit the highest heat radiation under pure combustion conditions, meaning in excess O_2 and in the absence of NO in the feed gas. The addition of NO to the reaction gas atmosphere depresses heat emission from the different materials in most cases. Heat reduction is also observed with decreasing O_2 contents in the feed gas, resulting in the absence of oxygen in the low values already discussed. This activity decline is very uniform for some of the samples, while other candidates fluctuate.

With the exception of the oxygen-free test segment, the Hopcalite benchmark is always located at the top of the activity

ranking lists, whereas several samples from groups (I) to (IV) offer activities superior to the Pt supported on Al_2O_3 reference catalyst. The mostly higher activities of both reference catalysts are expected since their specific surface areas are very large in comparison to all other materials in the library. This makes it all the more surprising that some nanopowders offer similar or slightly higher heat emissions than Pt/Al_2O_3 given their much lower surface areas.

When all diagrams are compared, it becomes obvious that the mixed-metal oxides from group (V) Co_xAl_{100-x}, (VI) Ni_xAl_{100-x}, and (VII) Ni_xCu_{100-x} demonstrated low activity under all reaction conditions used here. In addition, the mixed-metal oxides containing higher Co contents or mixed-metal oxides of Ni and Cu demonstrated a surprising cooling behavior under reaction atmospheres with low O_2 concentrations. Previous studies already showed that pure or supported oxides of cobalt[80−82] and copper[83−85] exhibit an appreciable capacity to reduce NO with propane or propene in the presence of excess O_2. However, these earlier results are not confirmed by our investigation. These results can presumably be explained by dissimilar test conditions and essential differences with regard to the catalyst preparation methods used resulting in completely different catalytic properties.

Note that cobalt (in particular Co_3O_4) and copper appear to be useful in improving sulfur poisoning resistance in NO_x storage and reduction (NSR) catalysts.[86] Furthermore, Co has been suggested as a promoter for platinum (oxidizing agent) in NSR catalysts because it improves NO_x storage and conversion efficiencies in these catalysts.[87,88] The storage of NO_x is an endothermic process which comprises the oxidation of NO to NO_2 over the oxidation agent followed by a subsequent adsorption of NO_2 by means of disproportion to form nitrates at the surface of a alkaline-earth metal-containing material (typically Ba).[89,90] Taking this into account, it is unlikely that NO_x storage processes are responsible for the cooling seen for the Ni_xCu_{100-x} and Co containing catalysts as an NO_x storage component like barium is absent in these catalysts. Additionally, the apparent cooling increases with reducing oxygen content in the feed gas, but the oxidation of NO (eq 4) usually proceeds under lean conditions, meaning under excess oxygen.

However, a more realistic explanation could be a reversible change in the emissivity characteristics of these compositions during the course of the measurement. For example, due to an alteration in oxidation states induced by a partial surface reduction of these materials with NO and propane, the applied emissivity correction is no longer correct, leading to "false negatives" in the obtained IR delta image.

The most interesting behaviors are those of materials from groups (I) to (IV), in particular the different mixtures of CeO_2 with ZrO_2 (group (II)), which provide the highest heat emissions of all examined oxides with the exception of the reference catalysts. However, a direct correlation of composition with catalytic activity is not reflected by the data, although higher ZrO_2 contents seem to have a positive effect. Apart from the ceria−zirconia solid solutions, the single oxides of Ce and Zr also exhibit comparatively high heat emissions.

In view of the already quite substantial research efforts in the application of ceria and related materials for catalysis, in particular for automobile exhaust gas conversion, these findings are not completely new.[14,91] For many years, ceria has been the chief oxygen storage component for three-way catalysts, and the mechanisms by which it works have been the subject of many studies.[92] Another important catalytic property of ceria is its ability to completely oxidize hydrocarbons along with CO and H_2. For these reasons particularly, the catalytic combustion of hydrocarbons on ceria has been studied for a long time. For example, total oxidation of parafins as well as unsaturated hydrocarbons on ceria can be achieved between 300 and 500 °C.[14]

A main disadvantage of ceria is its poor resistance to sintering. This is a major problem particularly for catalysts where specific surface areas should be as high as possible. Therefore, many attempts have been made to improve the sintering resistance of ceria-based catalysts by doping or mixing ceria with other oxides. An important breakthrough in this context was the use of zirconia as a dopant because zirconium ions can enter the ceria network without too much stress on the lattice, and therefore, solid solutions of ceria and zirconia with many different compositions have been synthesized successfully and characterized with regard to thermal stability, oxygen storage capacity, sintering resistance, and catalytic properties.[93]

Numerous studies concerning the catalytic combustion of volatile organic compounds[14,94−96] and the decomposition of NO_x[97,98] over ceria−zirconia catalysts have been reported in the catalysis literature, which emphasizes the general utility of these materials for environmental catalysis. Taking this into account, the results found in our investigation can be regarded as additional verification of previous studies, but it also demonstrates the applicability of liquid-feed flame spray pyrolysis as an appropriate synthesis method for ceria−zirconia catalysts.

As shown in the diagrams a, b, and c in Figure 7, the combination of CeO_2 or ZrO_2 with Al_2O_3 does not lead to drastic

(80) Yan, J.; Kung, M. C.; Sachtler, W. M. H.; Kung, H. H. *J. Catal.* **1997**, *172*, 178–186.
(81) Liotta, L. F.; Pantaleo, G.; Macaluso, A.; Di Carlo, G.; Deganello, G. *Appl. Catal. A* **2003**, *245*, 167–177.
(82) Horiuchi, T.; Fujiwara, T.; Chen, L.; Suzuki, K.; Mori, T. *Catal. Lett.* **2002**, *78*, 319–323.
(83) Bennici, S.; Gervasini, A.; Ravasio, N.; Zaccheria, F. *J. Phys. Chem. B* **2003**, *107*, 5168–5176.
(84) Bennici, S.; Carniti, P.; Gervasini, A. *Catal. Lett.* **2004**, *98*, 187–194.
(85) Metelkina, O. V.; Lunin, V. V.; Sadykov, V. A.; Alikina, G. M.; Bunina, R. V.; Paukshtis, E. A.; Fenelonov, V. B.; Derevyankin, A. Y.; Zaikovskii, V. I.; Schubert, U.; Ross, J. R. H. *Catal. Lett.* **2002**, *78*, 111–114.
(86) Clacens, J.-M.; Montiel, R.; Kochkar, H.; Figueras, F.; Guyon, M.; Beziat, J. C. *Appl. Catal. B* **2004**, *53*, 21–27.
(87) Vijay, R.; Snively, C. M.; Lauterbach, J. *J. Catal.* **2006**, *243*, 368–375.
(88) Vijay, R.; Hendershot, R. J.; Rivera-Jiménez, S. M.; Rogers, W. B.; Feist, B. J.; Snively, C. M.; Lauterbach, J. *Catal. Commun.* **2005**, *6*, 167–171.
(89) Fridell, E.; Skoglundh, M.; Westerberg, B.; Johansson, S.; Smedler, G. *J. Catal.* **1999**, *183*, 196–209.
(90) Hess, C.; Lunsford, J. H. *J. Phys. Chem. B* **2002**, *106*, 6358–6360.
(91) González-Velasco, J. R.; Gutiérrez-Ortiz, M. A.; Marc, J.-L.; Botas, J. A.; González-Marcos, M. P.; Blanchard, G. *Appl. Catal. B* **1999**, *22*, 167–178.
(92) Trovarelli, A. *Catal. Rev.* **1996**, *38*, 439–520.
(93) Di Monte, R.; Kaspar, J. *J. Mater. Chem.* **2005**, *15*, 633–648.
(94) de Rivas, B.; Gutiérrez-Ortiz, J. I.; López-Fonseca, R.; González-Velasco, J. R. *Appl. Catal. A* **2006**, *314*, 54–63.
(95) Díaz, E.; de Rivas, B.; López-Fonseca, R.; Ordóñez, S.; Gutiérrez-Ortiz, J. I. *J. Chromatogr. A* **2006**, *1116*, 230–239.
(96) Gutiérrez-Ortiz, J. I.; de Rivas, B.; López-Fonseca, R.; González-Velasco, J. R. *Appl. Catal. B* **2006**, *65*, 191–200.
(97) Adamowska, M.; Muller, S.; Da Costa, P.; Krzton, A.; Burg, P. *Appl. Catal. B* **2007**, *74*, 278–289.
(98) Silveira, E. B.; Perez, C. A. C.; Baldanza, M. A. S.; Schmal, M. *Catal. Today* **2008**, *133−135*, 555–559.

increases in activity. As might be expected, increasing Al_2O_3 contents greatly reduces catalytic activities. In particular, for compositions with ≥50 mol % Al_2O_3, the activities fall to very low levels compared to pure CeO_2 and pure ZrO_2. Given that LF-FSP produced materials along the CeO_x/Al_2O_3 and ZrO_2/Al_2O_3 tielines lead to core−shell materials where the alumina is coating crystals of ceria or zirconia or solid solutions thereof, we can easily imagine that gaseous access to the active components is limited. In the view of this result, it is not really surprising that combinations of all three oxides do not result in supplementary improvements in catalytic activity. Nevertheless, the ternary oxides with low Al_2O_3 contents demonstrate activities comparable to those provided by the binary Ce/Zr oxides.

An accompanying paper[99] suggests that the higher ZrO_2 contents actually contain significant amounts of the partially reduced species generally called zirconium suboxides (e.g., ZrO_{2-x} with some Zr^{3+}/Zr^{2+} ions). Furthermore, we recently reported that LF-FSP of compositions along the $CeO_2-Al_2O_3$ tieline produced solid-phase solutions at up to 5 mol % CeO_2, and at compositions up to 10 mol %, the materials consist primarily of the magnetoplumbite phase, $CeAl_{11}O_{18}$.[100] Thereafter, at higher CeO_2 contents, core−shell particles are observed with CeO_2 cores but with the shells containing considerable amounts of Ce^{3+} species probably as $CeAl_{11}O_{18}$. It is possible therefore to envision that, at low Al_2O_3 contents, the resulting shells contain considerable quantities of Ce^{3+} and possibly Zr^{3+}, which may contribute to the overall activity. Finally, given that the LF-FSP often produces kinetic rather than thermodynamic phases, it is also possible that even the "pure" $Ce_xZr_{1-x}O_2$ solid solutions actually may be better considered to exist as $Ce_xZr_{1-x}O_{2-z}$ partially reduced materials.

3. Catalyst Testing. Complementary to the above test runs, a set of experiments was run briefly to characterize the catalytic properties on stream by using propene instead of propane for reasons discussed below.

As noted above, numerous catalysts have been tested for reduction of NO with hydrocarbons. As of now, there are no catalysts that are robust and active enough to reduce the NO_x emissions of diesel engines with the onboard hydrocarbon fuel, which is the simplest and lowest cost solution to NO_x reduction. The ideal catalyst must operate over a wide temperature range, be resistant to poisoning by small amounts of SO_2 in the exhaust, be cheap, and have a long service life under high-temperature conditions. With these requirements in mind, and based on our initial survey, the catalytic activity of two $Ce_xZr_{1-x}O_2$ compositions toward simultaneous NO_x reduction and propene oxidation was investigated using conditions described in the Experimental Section. Figure 8 shows the results of a selective NO_x reduction/propene oxidation test made on 20 m^2/g of $Ce_{0.7}Zr_{0.3}O_2$ powder. These tests were run with propene for comparison with previous studies on three traditional sol−gel catalysts, made in the Gulari group at UM, as shown in Figure 9.[65]

While the specific peak activities of the catalysts shown in Figure 9 are higher than that of $Ce_{0.7}Zr_{0.3}O_2$ shown in Figure 8, all of the known catalysts in Figure 9 have significant limitations. For example, the activity window of the Pt/alumina catalyst runs from 150 to 300 °C and as such is too narrow for commercial use (diesel engines need catalysts that are active at 200−600 °C). The peak activities of silver and Cu-ZSM5 catalysts are

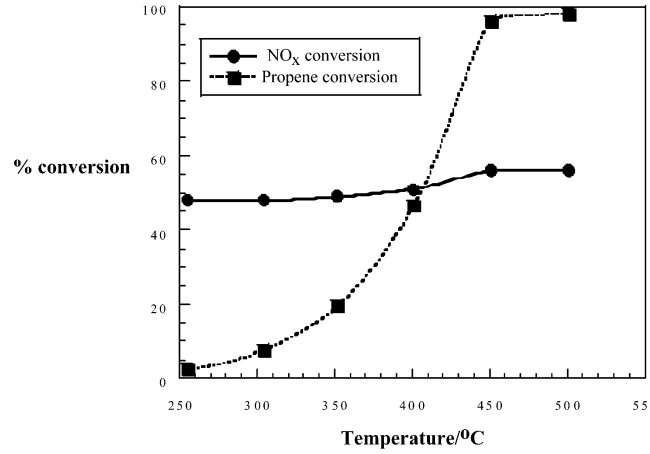

Figure 8. NO_x reduction/propene oxidation on 20 m^2/g of $Ce_{0.7}Zr_{0.3}O_2$ as a function of temperature. Propene oxidizes (>90% to CO_2) NO_x, reduces to N_2 (>99%) selectively.[65,66]

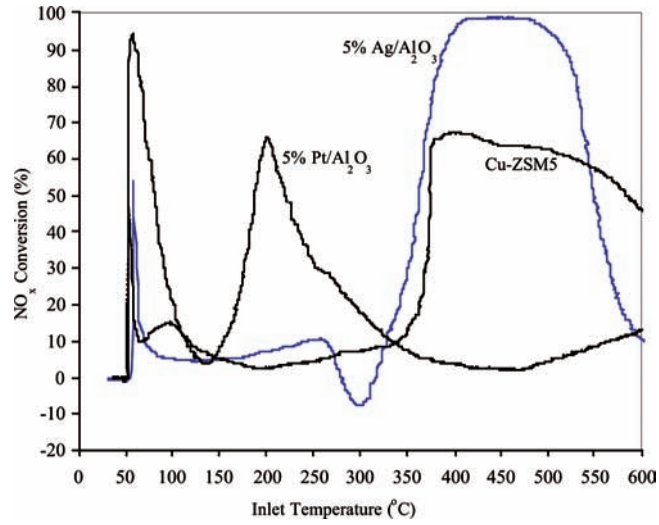

Figure 9. NO_x reduction activities of three of the most active and studied catalysts.[65,66]

reached only above 300 °C. Furthermore, Cu-ZSM5 catalyst is not stable in a humid atmosphere, while silver is deactivated by water as well as sulfur dioxide. $Ce_{0.7}Zr_{0.3}O_2$ is thermally very stable and has a very steady conversion rate from 250 °C (actually the window extends to below 200 °C) to 550 °C, ideally matching the diesel and lean-burn gasoline engine exhaust emission temperature windows. Sensitivity to water appears minimal, and conversion rates do not change significantly with temperature.

Of special interest is that $Ce_{0.7}Zr_{0.3}O_2$ by itself appears to be a better catalyst than a $Pt/Ce_{0.7}Zr_{0.3}O_2$ catalyst prepared from the same material (Figure 10). Finally, in addition to the catalyst's excellent behavior with NO_x, all of the propene used in the Figure 9 studies is oxidized at ≥430 °C, indicating a high degree of catalyst activity for control of hydrocarbon emissions, as well. Thus, it is likely that use of this same type of catalytic material in standard TWCs will also work well.

Conclusions/Outlook

The objective of the work described here was to couple the rapid sample output of LF-FSP for the production of high surface area, nonporous mixed-metal oxide nanopowders to high-throughput screening to demonstrate the utility of coupling

(99) Kim, M.; Laine, R. M. *J. Am. Chem. Soc.* **2009**, *131*, http://dx.doi.org/10.1021/ja9017545.
(100) Kim, M.; Hinklin, T. R.; Laine, R. M. *Chem. Mater.* **2008**, *20*, 5154–5162.

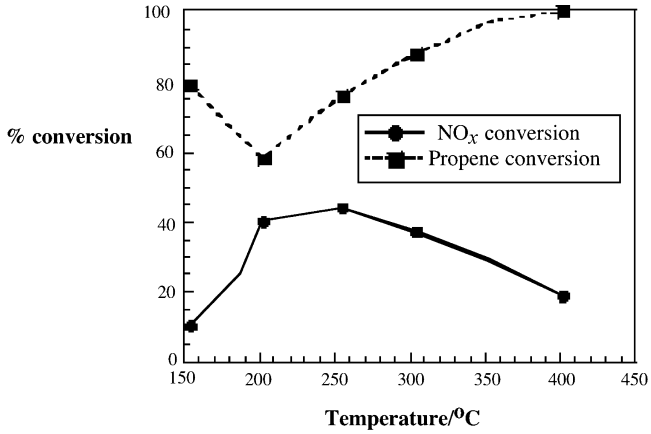

Figure 10. Selective NO_x reduction and propene oxidation activity of 0.5 wt % Pt on 20 m^2/g of $Ce_{0.7}Zr_{0.3}O_2$ nanopowder as a function of temperature.[65−67]

these two methods toward the preparation and screening of well-known as well as novel catalyst systems. We chose to study deNO_x catalysis as a means of screening a set of LF-FSP materials.

We find that this approach works extremely well to screen a wide variety of LF-FSP produced materials. Because LF-FSP produced nanopowders consist very often of kinetic rather than thermodynamic phases, it is possible to produce materials that are difficult to access or are completely inaccessible via traditional catalyst preparation methods. Indeed, our studies have identified a series of nano-$Ce_{1-x}Zr_xO_2$ and $Al_2O_3-Ce_{1-x}Zr_xO_2$ materials that offer surprisingly good activities for both NO_x reduction and propane/propene oxidation both in high-throughput screening studies and in continuous flow catalytic studies. Under the reaction conditions and with the model reductants, such as propane and propene, used in this paper, LF-FSP produced oxide catalysts offer activities comparable to traditional Pt/Al_2O_3 catalysts but without the addition of Pt. Thus, they are Pt-free, yet still active for extremely important emission control reactions, especially considering these are only first generation materials. For these oxide catalysts to be viable alternatives, further testing is needed using the real exhaust of a diesel engine and road conditions.

Improvements will no doubt come with further efforts to increase surface areas. Experiments will also be necessary to understand the long-term aging of these catalysts plus additional studies of compositional variations to optimize performance under conditions which are different than those of interest for the TWC systems. Finally, there is the potential opportunity to develop these catalysts for gas turbine engines which currently operate at temperatures of 1100−1300 °C, where simple noble metal catalysts react with typical support materials.[65−67]

With regard to compositional variation, we intend to combine the most active representatives of the two systems with variable contents of selected elements (single- and multielement doping) in order to seek out new catalyst lead compositions by means of combinatorial optimization circles. An additional interesting question is related to the impact of different morphologies within these systems as well as different particle sizes on the catalytic activity. In this context, the catalytic properties of the mixed-phase core−shell $CeO_2/ZrO_2/Al_2O_3$ particles with lower contents of Al_2O_3 will be further characterized, in particular, with regard to the influence of the CeO_x species in the Al_2O_3 shell.

Apart from that, the direct inkjet printing of ceramic suspensions has become a well-established method to prepare libraries of nanosized ceramic powders in the recent years.[101] Therefore, we are planning to incorporate this auspicious technique into our library generation procedures to accelerate our research.

Acknowledgment. The University of Michigan researchers would like to thank AFOSR (Contract No. F49620-03-1-0389) and a subcontract from UES Inc. (F074-009-0041/AF07-T009), Maxit Inc., Diamond Innovations Inc., and NSF for support of the LF-FSP synthesis work. We would also like to thank Dr. George W. Graham for helpful discussions on TWC catalysts in general and the results presented here.

Supporting Information Available: Additional tables. This material is available free of charge via the Internet at http://pubs.acs.org.

JA809134S

(101) Chen, L.; Zhang, Y.; Yang, S.; Evans, J. R. G. *Rev. Sci. Instrum.* **2007**, *78*, 072210–072216.